Local vibrational modes of substitutional Mg^{2+}, Ca^{2+}, and S^{2-} in zinc-blende and wurtzite II-VI semiconductors

M. Dean Sciacca, A. J. Mayur, N. Shin, I. Miotkowski, A. K. Ramdas, and S. Rodriguez
Department of Physics, Purdue University, West Lafayette, Indiana 47907-1396
(Received 25 July 1994; revised manuscript received 30 September 1994)

Localized vibrations of substitutional Mg^{2+}, Ca^{2+}, and S^{2-} in CdTe, ZnTe, and CdSe are observed as sharp absorption lines in the infrared and display as many lines as there are isotopes of the impurity, their intensities being proportional to their natural abundances. The lowering of the site symmetry from T_d in the zinc-blende CdTe and ZnTe to C_{3v} in the wurtzite CdSe causes the triply degenerate (Γ_5) mode in the former to split into a singlet (Γ_1) and a doublet (Γ_3) in the latter, the singlet and the doublet appearing only for the electric vector along the optic axis and normal to it, respectively. The features of the local mode are interpreted in terms of an anharmonic oscillator consistent with the site symmetry of the impurity. The evolution of the Mg^{2+} local mode from that in CdTe to that in ZnTe, as observed in a series of Mg doped $Cd_{1-x}Zn_xTe$ samples, provides insights into the variation of the local mode frequency or, equivalently, the Mg-Te force constant in the context of virtual crystal approximation. Their linewidths, however, can be correlated with the $x(1-x)$ disorder in the ternary. Ultrahigh resolution measurements of the Mg^{2+} local mode in ZnTe and CdSe reveal fine structures originating in the isotopic disorder of the nearest neighbor Te and Se, respectively.

I. INTRODUCTION

As is well known, an impurity with an atomic mass significantly smaller than those of the constituent atoms of an otherwise perfect host crystal, exhibits a vibrational mode with a frequency higher than those of the normal modes of the perfect crystal; the displacements of the atoms in such a mode are strongly peaked at the impurity site—hence the nomenclature "local mode."[1,2] In the tetrahedrally coordinated II-VI semiconductors, one encounters many examples of impurities which exhibit such characteristic local modes. Consider, for example, a dilute concentration of Mg randomly replacing Cd in CdTe. The significantly smaller mass of Mg results in a local mode as reported by Oh *et al.*[3] in a comprehensive study of the infrared and Raman spectra of the ternary $Cd_{1-x}Mg_xTe$ and the quaternary $Cd_{1-x-y}Mg_xMn_yTe$; in this investigation, the evolution of the local mode into the collective, zone-center, "MgTe-like" mode is clearly observed. Other examples of local modes in zinc-blende II-VI's reported in the literature are those of Be^{2+} in ZnTe, ZnSe, and ZnS[4], of Be^{2+} in CdTe[5], of Mg^{2+} in CdTe,[3,6] and of S^{2-}, Be^{2+}, and Mg^{2+} in $Zn_xCd_{1-x}Te$.[7] The local modes of Be^{2+} in CdSe and CdS reported by Manabe *et al.*,[8] illustrate the effect of lowering the site symmetry from T_d in the zinc blende to C_{3v} associated with the wurtzite structure of CdSe and CdS. When the light impurity is present in extreme dilution, the local mode observed in the infrared clearly shows the dependence of its frequency on the isotopic mass.[3,6]

We report in the present paper the results of an experimental study of the local modes of Mg^{2+}, Ca^{2+}, and S^{2-} in CdTe, ZnTe, $Cd_{1-x}Zn_xTe$, and CdSe investigated in the infrared with a Fourier transform spectrometer. The results are interpreted in terms of the vibrational levels of a light impurity confined to an anharmonic potential consistent with its site symmetry.

II. THEORETICAL CONSIDERATIONS

The localized vibration of a light impurity, of mass M, in a host crystal can be modeled as an oscillator confined to an anharmonic potential consistent with the site symmetry of the impurity. A substitutional impurity in a zinc-blende lattice has T_d site symmetry. It has been shown by Elliott *et al.*[9] that the potential of an anharmonic oscillator with T_d symmetry, referred to the cubic axes (x,y,z) is

$$V(T_d) = \frac{k}{2}(x^2+y^2+z^2) + B(xyz) + D_1(x^4+y^4+z^4) + D_2(y^2z^2+z^2x^2+x^2y^2) + \cdots, \quad (1)$$

where k, B, D_1, and D_2 are parameters to be determined by theoretical fits to the experimental data. Treating the cubic term to second order and the quartic terms to first order in perturbation theory, the energy levels are given by

$$E_N = \hbar\sqrt{\frac{k}{M'}}(N+3/2) - \frac{\hbar^2}{24k^2M'}\lambda B^2 + \frac{\hbar^2}{4kM'}(\mu_1 D_1 + \mu_2 D_2), \quad (2)$$

where $N = 0,1,2,\ldots$ and $M' = MM_L/(M+M_L)$ is

the reduced mass of the oscillator incorporating a *lattice interaction mass* M_L to take into account empirically the small motion of the surrounding lattice [M_L is also treated as a fitting parameter and is found to be between one and four times the mass of a nearest neighbor (NN) atom[10]]. The values for μ_1, μ_2, and λ as deduced from perturbation theory by Elliot *et al.*[9] along with the symmetry of the states in the notation of Koster *et al.*[11] are given in Table 3 of Newman.[2] The energy levels are shown schematically in Fig. 1 along with the irreducible representations to which they belong. The electric dipole in T_d transforms as Γ_5 and hence electric dipole transitions originating from the ground state, which belongs to Γ_1, can only terminate at states having $\Gamma_1 \otimes \Gamma_5 = \Gamma_5$ symmetry. There is one such $\Gamma_1 \rightarrow \Gamma_5$ electric dipole allowed transition in the fundamental and one in the second harmonic.

A substitutional impurity and the associated anharmonic potential in a wurtzite lattice possess C_{3v} symmetry. In a C_{3v} environment it is advantageous to change from the (x, y, z) coordinate system to (ξ, η, ζ) coordinates in which the ζ axis is parallel to the [111] crystallographic c axis, the ξ and η axes are parallel to $[1\bar{1}0]$ and $[11\bar{2}]$, respectively. Newman[2] has formulated the general C_{3v} potential referred to the (ξ, η, ζ) coordinate system and Manabe *et al.*[12] have calculated the energy levels treating the cubic terms to second order in perturbation theory. It has been suggested by Newman that a better approximation would be to add the quartic terms appropriate to T_d symmetry to the general C_{3v} potential and treat the former to first order and the latter to second order in perturbation theory. Following this prescription, the potential can be written as

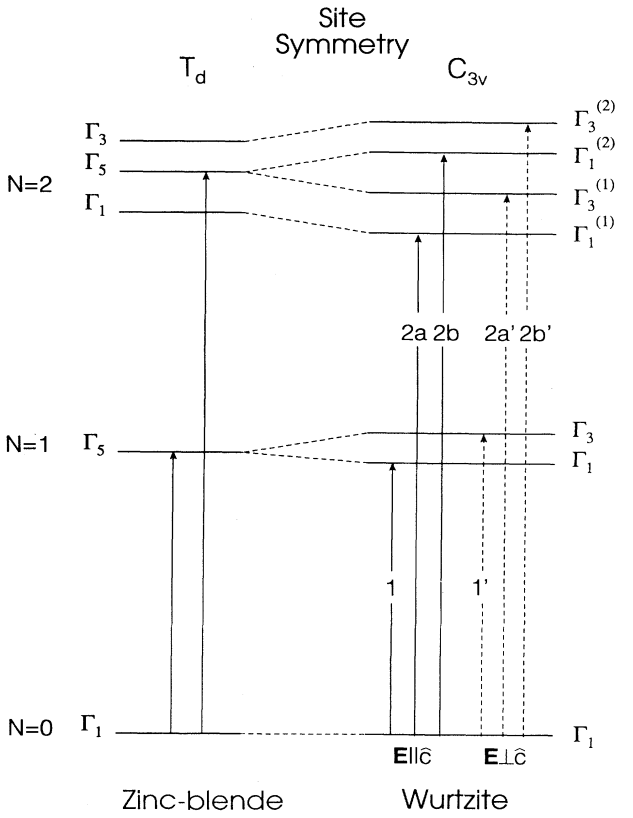

FIG. 1. Schematic energy level diagram of an anharmonic oscillator with T_d and C_{3v} symmetry. The electric dipole allowed transitions are designated by vertical arrows, according to the selection rules described in the text.

$$V(C_{3v}) = \frac{k_\parallel}{2}\zeta^2 + \frac{k_\perp}{2}(\xi^2+\eta^2) + B_1\zeta^3 + B_2\zeta(\xi^2+\eta^2) + B_3[\xi\eta^2 - (1/3)\xi^3] + C_1\zeta^4 + C_2\zeta^2(\xi^2+\eta^2) + C_3\zeta\xi[\eta^2 - (1/3)\xi^2] + C_4(\xi^2+\eta^2)^2, \quad (3)$$

where $k_\parallel$ and $k_\perp$ are the force constants parallel and perpendicular to the ζ axis ($\hat{c}$), respectively, $k_\parallel$, $k_\perp, \ldots, C_4$ being determined by fitting the theory to the experimentally observed energies of the fundamentals and the second harmonics. The energy levels calculated from perturbation theory are

$$E(N_\xi, N_\eta, N_\zeta) = \hbar\sqrt{\frac{k_\perp}{M'}}(N_\xi + N_\eta + 1) + \hbar\sqrt{\frac{k_\parallel}{M'}}(N_\zeta + 1/2) - \frac{\hbar^2}{8M'}\left(\frac{\alpha B_1^2}{k_\parallel^2} + \frac{\beta B_1 B_2}{k_\parallel^{3/2}k_\perp^{1/2}} + \frac{\gamma B_2^2}{k_\parallel k_\perp} + \frac{\delta B_2^2}{k_\parallel^{1/2}k_\perp(2k_\perp^{1/2}+k_\parallel^{1/2})} + \frac{\epsilon B_2^2}{k_\parallel^{1/2}k_\perp(2k_\perp^{1/2}-k_\parallel^{1/2})} + \frac{\lambda B_3^2}{k_\perp^2}\right) + \frac{\hbar^2}{4M'}\left(\frac{\mu_1 C_1}{k_\parallel} + \frac{\mu_2 C_2}{k_\parallel^{1/2}k_\perp^{1/2}} + \frac{\mu_3 C_3}{k_\parallel^{1/4}k_\perp^{3/4}} + \frac{\mu_4 C_4}{k_\perp}\right), \quad (4)$$

where N_ξ, N_η, $N_\zeta = 0, 1, 2, \ldots$, and M' is again the reduced mass of the oscillator with M_L being treated as a fitting parameter. Table I lists the values of $\alpha, \beta, \ldots, \lambda$ and the μ_i's, the symmetry of the states and the wave functions, $|N_\xi, N_\eta, N_\zeta\rangle$. The lowering of the site symmetry splits each triply degenerate Γ_5 level of T_d into a singlet Γ_1 and a doublet Γ_3 of C_{3v} as shown in Fig. 1. The component of the electric dipole along the $\hat{c}$ transforms as Γ_1 and that perpendicular to $\hat{c}$ as Γ_3. Therefore, $\Gamma_1 \rightarrow \Gamma_3$ transitions are allowed for the electric vector of the incident radiation $\mathbf{E} \perp \hat{c}$, whereas the transitions $\Gamma_1 \rightarrow \Gamma_1$ are allowed for $\mathbf{E} \parallel \hat{c}$.

III. EXPERIMENTAL RESULTS AND DISCUSSION

The absorption spectra were recorded using a BOMEM DA.3 Fourier transform spectrometer.[13] Typically, 0.5

TABLE I. Wave functions and anharmonic parameters for a local mode oscillator in trigonal (C_{3v}) symmetry. The superscripts in brackets are labels used to identify states with the same symmetry and N, as shown in Fig. 1.

N	Wave functions	Symmetry	μ_1	μ_2	μ_3	μ_4	α	β	γ	δ	ϵ	λ
0	$\|0,0,0\rangle$	Γ_1	3	2	0	8	11	12	4	4	0	8/9
1	$\|0,0,1\rangle$	Γ_1	15	6	0	8	71	36	4	8	4	8/9
1	$\|1,0,0\rangle; \|0,1,0\rangle$	Γ_3	3	4	0	24	11	24	16	8	0	56/9
2	$\|0,0,2\rangle$	$\Gamma_1^{(1)}$	39	10	0	8	191	60	4	12	8	8/9
2	$\|1,0,1\rangle; \|0,1,1\rangle$	$\Gamma_3^{(1)}$	15	12	0	24	71	72	16	16	8	56/9
2	$\frac{1}{\sqrt{2}}(\|2,0,0\rangle + \|0,2,0\rangle)$	$\Gamma_1^{(2)}$	3	6	0	56	11	36	36	16	-4	248/9
2	$\frac{1}{\sqrt{2}}(\|2,0,0\rangle - \|0,2,0\rangle)$; $-\|1,1,0\rangle$	$\Gamma_3^{(2)}$	3	6	0	48	11	36	36	12	0	80/9
3	$\frac{1}{2}(\|3,0,0\rangle - \sqrt{3}\|1,2,0\rangle)$	$\Gamma_1^{(1)}$	3	8	0	80	11	48	64	16	0	80/9
3	$\frac{1}{2}(\|0,3,0\rangle - \sqrt{3}\|2,1,0\rangle)$	Γ_2	3	8	0	80	11	48	64	16	0	80/9
3	$\frac{1}{2}(\sqrt{3}\|3,0,0\rangle + \|1,2,0\rangle)$; $\frac{1}{2}(\|2,1,0\rangle + \sqrt{3}\|0,3,0\rangle)$	$\Gamma_3^{(1)}$	3	8	0	96	11	48	64	24	-8	416/9
3	$\frac{1}{\sqrt{2}}(\|2,0,1\rangle + \|0,2,1\rangle)$	$\Gamma_1^{(2)}$	15	18	0	56	71	108	36	28	8	248/9
3	$\frac{1}{\sqrt{2}}(\|2,0,1\rangle - \|0,2,1\rangle)$; $-\|1,1,1\rangle$	$\Gamma_3^{(2)}$	15	18	0	48	71	108	36	24	12	80/9
3	$\|0,0,3\rangle$	$\Gamma_1^{(3)}$	75	14	0	8	371	84	4	16	12	8/9
3	$\|1,0,2\rangle; \|0,1,2\rangle$	$\Gamma_3^{(3)}$	39	20	0	24	191	120	16	24	16	56/9

cm^{-1} resolution and 50 coadditions proved more than adequate. The detector was a composite silicon bolometer[14] operating at 4.2 K. Absorption spectra were recorded with the samples cooled to 5 K in a Janis 10DT Supervaritemp optical cryostat with polypropylene windows.[15] The experimental details regarding crystal growth will be reported elsewhere.[16]

A. Mg^{2+}, Ca^{2+}, and S^{2-} in CdTe and ZnTe: T_d site symmetry

As is well known, both CdTe and ZnTe crystallize in the zinc-blende (T_d^2) structure. Therefore, an impurity substitutionally replacing either the cation (Mg^{2+} or Ca^{2+} for Cd^{2+} or Zn^{2+}) or the anion (S^{2-} for Te^{2-}), has T_d site symmetry. As shown in Fig. 1, for each isotope of the impurity we expect a single electric dipole transition as a fundamental and as a second harmonic, with intensities of the absorption peaks due to each isotope being proportional to its isotopic abundance. In addition, the lighter the isotope, the higher its vibrational frequency. Magnesium has three isotopes, ^{24}Mg being approximately eight times more abundant than ^{25}Mg and ^{26}Mg. Thus one expects three sharp absorption lines at frequencies above the reststrahlen, with the highest frequency line approximately eight times stronger than the other two lines. As is typical of transitions between vibrational states, the local modes sharpen as the temperature is lowered from room temperature to, say, liquid nitrogen temperature (77 K), below which the width is relatively temperature independent.

In displaying the spectra of the local modes of substitutional impurities, it is instructive to subtract the background due to the pure host, emphasizing only the features due to the substitutional impurities. Such spectra are displayed in Fig. 2, where we present results on (a) Mg^{2+}, (b) Ca^{2+}, and (c) S^{2-} in CdTe. One can now easily deduce the peak positions of the local modes and their intensities (integrated areas) using a standard curve-fitting procedure. The deconvoluted areas under each peak (in percent) for ^{24}Mg, ^{25}Mg, and ^{26}Mg are 79.4, 9.7, and 10.9, respectively, in good agreement with the natural isotopic abundances[17] of 78.99, 10.00 and 11.01, providing confirmation of our assignment. Similarly, the local mode features associated with Ca^{2+} and S^{2-} in CdTe have also been identified and confirmed. The peak positions of the fundamentals of local modes as well as their second harmonics in CdTe are listed in Table II. In order to uniquely deduce the parameters for the T_d site symmetry introduced in Eq. (2) by appealing to the experimentally observed transitions, it is necessary to know the transition energy of the third harmonic. The tenfold degeneracy of the $N = 3$ level of an isotropic oscillator is lifted in the presence of a T_d potential and resolved into $\Gamma_1 + \Gamma_4 + 2\Gamma_5$; thus two electric dipole allowed third harmonics are expected. Such transitions were indeed observed for ^{24}Mg in $Cd_{0.95}Mg_{0.05}Te$ at 750.2 cm^{-1} and 761.1 cm^{-1}. We have also observed the fundamentals and the second harmonics of the local modes of Mg^{2+} and S^{2-} in ZnTe, whose energies are listed in Table II. The second harmonics of the local mode, which are observed only at a sufficiently high impurity concentration ($\sim 10^{20}$ cm^{-3}), occur at slightly less than twice the local mode frequency. Due to their relative weakness, signatures associated with some of the less abundant isotopes could not be observed.

It is interesting to note that the fundamental transition energies in ZnTe are $\sim$19 cm^{-1} higher than the corresponding transition energies in CdTe. A similar 19 cm^{-1} shift has also been observed for the local modes of $3d$-transition metal ions when the host is changed from

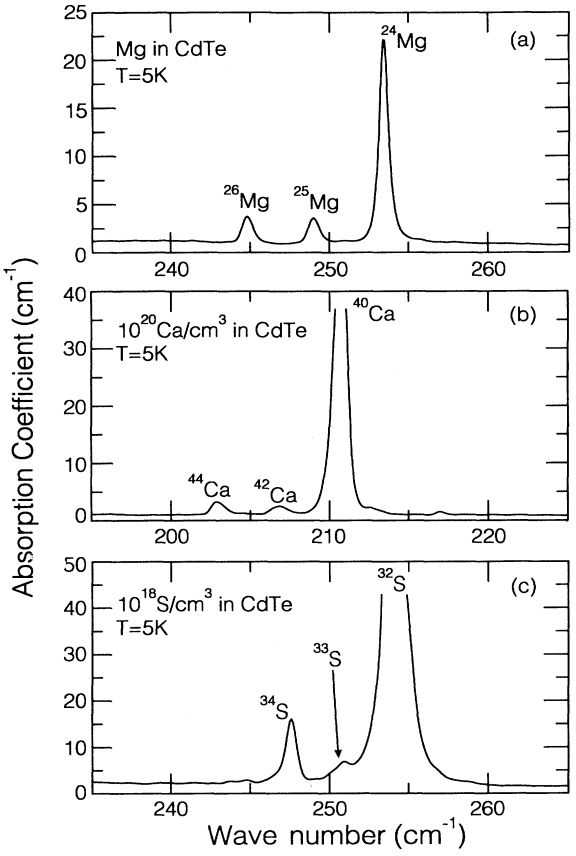

FIG. 2. The absorption spectrum of (a) Mg^{2+} local mode in CdTe, (b) Ca^{2+} local mode in CdTe, and (c) S^{2-} local mode in CdTe. Note the CdTe background has been subtracted.

CdTe to ZnTe.[18] The effect of the host on the local mode frequency is discussed in more detail in a later section.

With the plausible assumption that the parameters in Eq. (2) are independent of the mass of the isotope, they can now be determined by fitting the experimentally observed energies to the theory. The best fit values for the parameters for Mg^{2+} in CdTe, deduced from a nonlinear least-squares method, are listed in Table III. These values yield transition energies in agreement with those observed within the experimental uncertainty of 0.05 cm^{-1}. Sparsity of data prevented a similar analysis for Ca^{2+} and S^{2-} in CdTe as well as Mg^{2+} and S^{2-} in ZnTe. Although the inclusion of the D_1 and D_2 quartic terms in Eq. (2) is a desirable refinement, a fit with just M_L, the quadratic k and cubic B terms to the fundamental and second harmonic for CdTe:Mg^{2+} yields values for M_L, k, and B, which can predict the third harmonics to within 2 cm^{-1}. The parameters M_L, k, and B thus deduced for Ca^{2+} and S^{2-} in CdTe and Mg^{2+} and S^{2-} in ZnTe are listed in Table III. With these values for k and B the predicted positions of the third harmonics are 623.5 cm^{-1} and 635.4 cm^{-1} for ^{40}Ca in CdTe; 758.1 cm^{-1} and 764.2 cm^{-1} for ^{32}S in CdTe; 806.9 cm^{-1} and 820.9 cm^{-1} for ^{24}Mg in ZnTe; and 807.9 cm^{-1} and 822.6 cm^{-1} for ^{32}S in ZnTe.

TABLE II. The energies (in cm^{-1}) of the local modes of Mg^{2+}, Ca^{2+}, and S^{2-} in CdTe and ZnTe. The energies of the third harmonics in CdTe:Mg^{2+} are listed in the text.

	CdTe		ZnTe	
Isotope	Fundamental	Second harmonic	Fundamental	Second harmonic
^{24}Mg	253.3	505.3	272.3	542.9
^{25}Mg	248.9	496.5	267.6	533.6
^{26}Mg	244.7	488.2	263.3	524.9
^{40}Ca	210.6	419.9		
^{42}Ca	206.8			
^{44}Ca	202.8			
^{32}S	254.1	507.6	272.7	543.8
^{33}S	250.7			
^{34}S	247.5	494.1	265.7	

B. Mg^{2+} in CdSe: C_{3v} site symmetry

As shown in Fig. 1, the effect of lowering the site symmetry of the substitutional impurity from T_d in the zinc-blende CdTe and ZnTe to C_{3v} in CdSe, with C_{6v}^4 space group symmetry, is to split each triply degenerate (Γ_5) level into a singlet (Γ_1) and a doublet (Γ_3), with the former appearing in infrared absorption only for $\mathbf{E} \parallel \hat{c}$ and the latter only for $\mathbf{E} \perp \hat{c}$. Figure 3 shows the absorption spectra of CdSe:Mg for $\mathbf{E} \parallel \hat{c}$ (upper) and $\mathbf{E} \perp \hat{c}$ (lower) in the spectral range 225–325 cm^{-1}. In each polarization, the three sharp lines labeled ^{24}Mg, ^{25}Mg, and ^{26}Mg are the classic signature due to the Mg^{2+} local mode, the lines for $\mathbf{E} \parallel \hat{c}$ being assigned to transition 1 and those for $\mathbf{E} \perp \hat{c}$ to transition 1′ of Fig. 1 for each Mg isotope. The local mode frequencies for $\mathbf{E} \perp \hat{c}$ are shifted to higher energies with respect to those for $\mathbf{E} \parallel \hat{c}$, thus determining the order of the energy levels of the fundamental with excited states in which the doublet (Γ_3) lies above the singlet (Γ_1). The frequencies of these local mode lines are listed in Table IV. The origin of the two sharp lines labeled with a question mark in each polarization is as yet undetermined. These lines at 270.7 cm^{-1} for $\mathbf{E} \parallel \hat{c}$ and at 271.4 cm^{-1} for $\mathbf{E} \perp \hat{c}$ are observed in all the seven CdSe:Mg samples studied.

Consistent with the electric dipole allowed transitions for the second harmonic shown in Fig. 1, a pair of lines are observed in each polarization for each of the three Mg isotopes. From the positions of these lines which are listed in Table IV, one can order the energy levels corresponding to the second harmonic as shown in Fig. 1.

Again in order to uniquely determine all the parameters in Eq. (4), one requires the energies of the third harmonics. However, by appealing to the small effect of the quartic terms observed for T_d, only the quadratic $k_{\parallel}$ and $k_{\perp}$, the cubic B_1, B_2, and B_3 terms and M_L are used to fit Eq. (4) to the eighteen experimentally observed frequencies. The fitting algorithm used for the zinc blende was again employed to deduce the values of the parameters listed in Table III. The agreement between the experimental and theoretical transition energies is within 0.2 cm^{-1}. The importance of the quartic terms can be

TABLE III. The values of the parameters in Eqs. (2) and (4) deduced from theoretical fits to the experimental data. For Mg^{2+} in CdSe, $B_1B_2 < 0$.

	CdTe			ZnTe			CdSe
T_d parameters	Mg^{2+}	Ca^{2+}	S^{2-}	Mg^{2+}	S^{2-}	C_{3v} parameters	Mg^{2+}
k (10^4 dyn/cm)	8.079	8.530	10.93	9.074	12.50	$k_{\|}$ (10^4 dyn/cm)	9.315
						$k_{\perp}$ (10^4 dyn/cm)	9.167
$\|B\|$ (10^{13} erg/cm^3)	1.097	2.467	2.142	2.275	3.753	$\|B_1\|$ (10^{12} erg/cm^3)	4.806
D_1 (10^{20} erg/cm^4)	-1.593					$\|B_2\|$ (10^{12} erg/cm^3)	1.387
D_2 (10^{19} erg/cm^4)	9.007					$\|B_3\|$ (10^{12} erg /cm^3)	9.374
M_L (10^2 amu)	1.681	1.648	2.660	1.413	2.344	M_L (10^2 amu)	0.987

established by comparing future experimental observation of the third harmonic with the positions predicted by the above parameters.

C. Mg^{2+} in $Cd_{1-x}Zn_xTe$: Effect of the host lattice

In addition to the role of the site symmetry of the impurity (T_d in zinc blende and C_{3v} in wurtzite) in its local mode, it is equally, if not more interesting, to study the consequence of changing the impurity-NN bond length, while maintaining the NN species and site symmetry. The zinc-blende II-VI ternary alloys accessible over a wide composition range with a continuously tunable lattice constant offer an ideal system for such experiments. In addition, such a study allows one to address the effect of the host disorder on the local modes. Since $Cd_{1-x}Zn_xTe$ is accessible in the zinc-blende phase over the entire composition range $0 \leq x \leq 1$, we have studied the evolution of the Mg^{2+} local mode in this ternary, from 253.3 cm^{-1} in CdTe to 272.3 cm^{-1} in ZnTe.

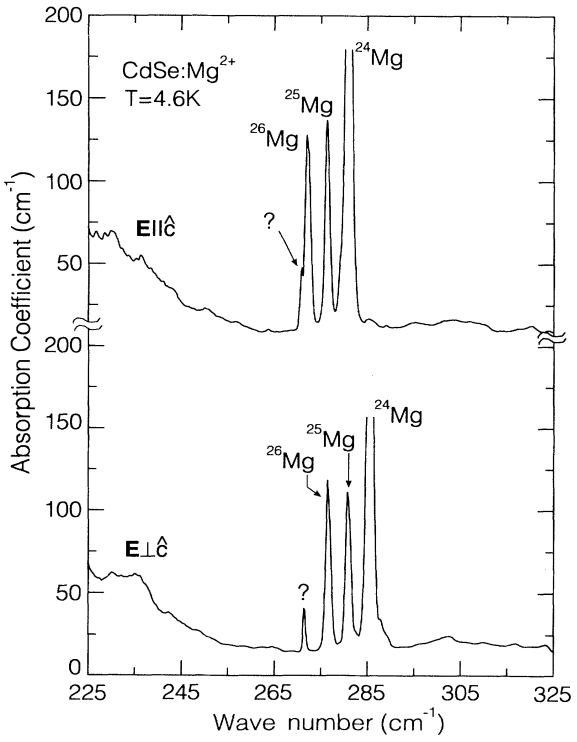

FIG. 3. The absorption spectrum of the Mg^{2+} local mode in CdSe for $\mathbf{E} \parallel \hat{c}$ (top) and $\mathbf{E} \perp \hat{c}$ (bottom), where $\mathbf{E}$ is the electric vector of the incident radiation and $\hat{c}$ is the optic axis. The lines labeled with a question mark in each polarization are of undetermined origin.

A series of $Cd_{1-x}Zn_xTe$ crystals doped with a nominal Mg^{2+} concentration of 10^{19}/cm^3 were specially grown for establishing the effect of the host on the local mode. The solid circles in Fig. 4(a) represent the ^{24}Mg local mode frequency observed in these crystals whose composition was determined by microprobe measurements. In the spirit of virtual crystal approximation (VCA), the *average* force constant characterizing the local mode of Mg^{2+} in the ternary $Cd_{1-x}Zn_xTe$ host can be expressed as $k = k_{Cd}(1-x) + k_{Zn}x$, namely, the weighted average of the force constants of the local mode in CdTe (k_{Cd}) and that in ZnTe (k_{Zn}); one can thus account for the increase in the Mg^{2+} local mode frequency with increasing x. The solid line in Fig. 4(a), which is constrained to pass through the end points represents the local mode frequency as a function of x calculated on the basis of these considerations. For $0.1 < x < 0.9$, the local modes are broadened to such an extent that the structure associated with the Mg isotopes is obscured; in such cases the peak position of the single broad absorption line was assumed to be the frequency of the dominant ^{24}Mg local mode. However, this peak position is lower than the actual ^{24}Mg local mode frequency due to the presence of the underlying ^{25}Mg and ^{26}Mg local modes, and may account for the small deviation of the assumed frequencies from the solid line. It would be preferable to study the local modes of a monoisotopic element, since the peak positions and the linewidths will then be more clearly defined. Such a study of the local modes of Ca^{2+} in $Cd_{1-x}Zn_xTe$ is being carried out since Ca consists of 97% ^{40}Ca.

Figure 4(b) shows the dependence of the full width at half maximum (FWHM) of the ^{24}Mg local mode absorption line as a function of x. If V_{Cd} and V_{Zn} are the potentials characterizing the Mg^{2+} local oscillator in CdTe and ZnTe, respectively, then, again in the spirit of VCA, the Mg^{2+} local mode in the alloy $Cd_{1-x}Zn_xTe$ is subject to an average field,

$$V = (1-x)V_{Cd} + xV_{Zn}. \quad (5)$$

This is not strictly true because a Mg atom having mainly

TABLE IV. The energies of the fundamental and second harmonic (in cm^{-1}) of the Mg^{2+} local mode in CdSe. The labels in brackets identify the optical transitions in Fig. 1.

	$\mathbf{E} \parallel \hat{c}$		$\mathbf{E} \perp \hat{c}$	
Isotope	Fundamental	Second harmonic	Fundamental	Second harmonic
^{24}Mg	280.9 (1)	566.8 (2b)	285.5 (1′)	570.8 (2b′)
		557.7 (2a)		566.2 (2a′)
^{25}Mg	276.2 (1)	557.7 (2b)	280.7 (1′)	561.6 (2b′)
		549.0 (2a)		557.3 (2a′)
^{26}Mg	271.9 (1)	549.0 (2b)	276.4 (1′)	552.9 (2b′)
		540.8 (2a)		548.6 (2a′)

a Cd environment experiences V_{Cd}, whereas that with mainly a Zn environment experiences V_{Zn}. Deviations from V can then be viewed as perturbations given by

$$V_{Cd} - V = x(V_{Cd} - V_{Zn}), \tag{6}$$

and

$$V_{Zn} - V = (1 - x)(V_{Zn} - V_{Cd}). \tag{7}$$

With the assumption that the randomly distributed Mg atoms are independent oscillators, the lifetime of the local mode is inversely proportional to the sum of the squares of the perturbations, so that one expects

$$\text{FWHM} \propto (1 - x)(V_{Cd} - V)^2 + x(V_{Zn} - V)^2, \tag{8}$$

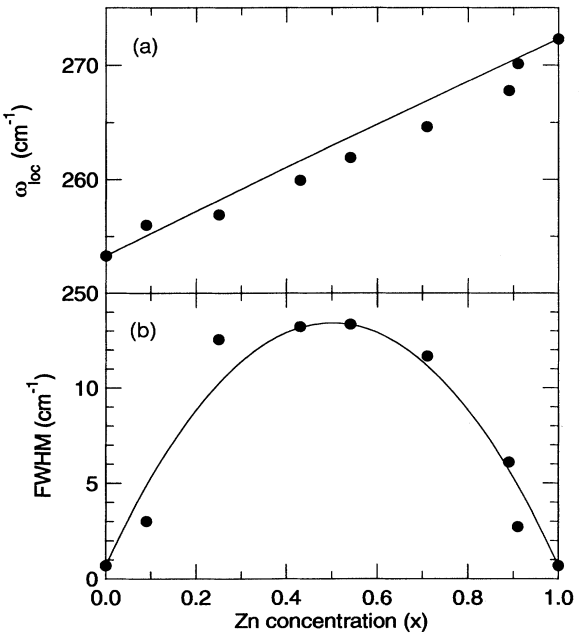

FIG. 4. (a) Plot of the local mode frequency (ω_{loc}) of ^{24}Mg in $Cd_{1-x}Zn_xTe$ as a function of Zn concentration. The full circles are the experimentally observed line positions and the line represents their dependence on x according to a model in which the Mg-Te force constant varies linearly with x. (b) The full width at half maximum (FWHM) of the ^{24}Mg local mode in $Cd_{1-x}Zn_xTe$ as a function of x. The curve represents a fit to the FWHM vs x on the basis of the theory in which it is proportional to $x(1 - x)$.

$(1 - x)$ and x being the probabilities for the Mg atom being in a Cd and a Zn environment, respectively. Using Eqs. (6) and (7) in Eq. (8), one finds[19]

$$\text{FWHM} \propto (V_{Cd} - V_{Zn})^2 x(1 - x). \tag{9}$$

The above discussion is clearly oversimplified in representing the departures from V. In addition, the energy shifts due to the perturbations have been ignored, the entire broadening being attributed to the lifetime effect. Alternatively, one could view the disorder associated with the alloy as producing corresponding fluctuations in the Mg-Te bond lengths and hence leading to associated frequency shifts of the Mg^{2+} local mode. Cai and Thorpe[20] have deduced that the NN bond length distribution function for tetrahedrally coordinated semiconductor alloys has a FWHM proportional to $x(1 - x)$ and hence one could, in turn, correlate it with the FWHM of the Mg^{2+} local mode. The relative importance of the "lifetime" and "bond length fluctuation" as factors influencing the FWHM of the local mode is not clear. The solid line in Fig. 4(b) represents a nonlinear least-squares fit of FWHM=$0.7+cx(1 - x)$ cm^{-1}, with c=51, which is constrained to pass through the end points. The 0.7 cm^{-1} FWHM of the ^{24}Mg local mode in CdTe and ZnTe is the NN Te isotope disorder limited width and is discussed in the next section.

IV. CONCLUDING REMARKS

The present investigation of localized vibrations in the II-VI's highlights the power of infrared spectroscopy as a means of characterizing electrically inactive foreign impurities in a concentration range not typically accessible to Raman spectroscopy. The sharpness of the spectral features on the one hand, and the high resolution available with Fourier transform infrared spectroscopy on the other, permits the isotopic character of the impurity to be fully exposed. In contrast, at high concentrations, where Raman spectroscopy proves to be more useful, the localized character gives way to collective modes in which the *average* isotopic mass is relevant. It is precisely at these higher concentrations that the local mode picture is replaced by a multimode behavior appropriate for II-VI ternary and quaternary alloys.[3,21,22]

The local symmetry of the neutral impurity is revealed in the infrared spectrum as a splitting of the triply de-

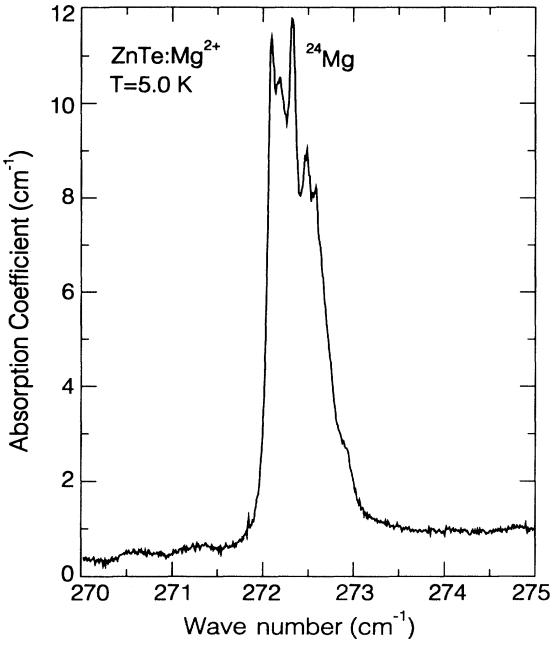

FIG. 5. Fine structure of the local mode of ^{24}Mg in ZnTe recorded with a 0.02 cm^{-1} resolution showing the effect of the isotopic disorder in the four NN Te's.

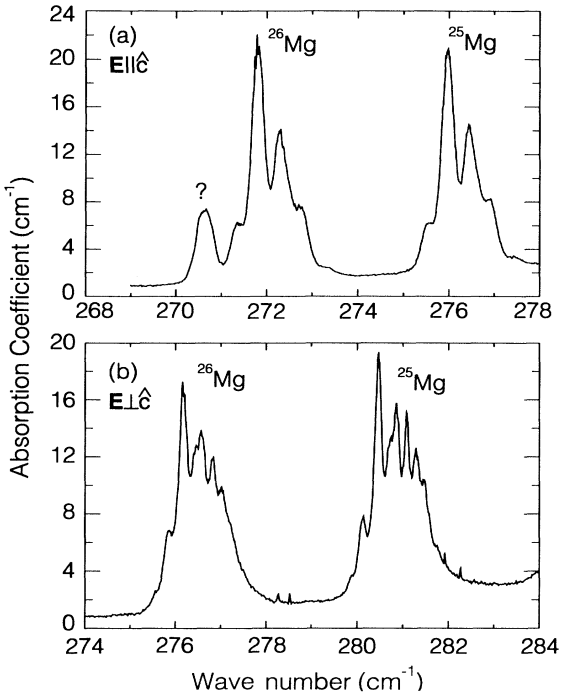

FIG. 6. Fine structure of the local modes of ^{25}Mg and ^{26}Mg in CdSe for $\mathbf{E} \parallel \hat{c}$ (a) and $\mathbf{E} \perp \hat{c}$ (b) recorded at 0.02 cm^{-1} resolution and 5 K.

generate mode (Γ_5) in T_d site symmetry into a singlet (Γ_1) and a doublet (Γ_3) in C_{3v} site symmetry along with the characteristic polarization effects. In this context, a study of the effects of uniaxial stress would be particularly useful.[5,23] The theory of localized vibrations predicts the occurrence of gap modes,[1] provided the light impurity replaces the heavier of the two constituents in a binary, as is the case for S^{2-} in CdTe and ZnTe and Mg^{2+} in CdSe. Indeed, we have observed such gap modes of S^{2-} in CdTe and ZnTe at 106.1 cm^{-1} and 144.6 cm^{-1}, respectively. Due to the uniaxial symmetry of CdSe, two gap modes of Mg^{2+} occur, one at 143.4 cm^{-1} and the other at 144.6 cm^{-1} for $\mathbf{E} \parallel \hat{c}$ and $\mathbf{E} \perp \hat{c}$, respectively.

In the ternary $Cd_{1-x}Zn_xTe$, the evolution of the Mg^{2+} local mode over the entire composition range has been observed in the present investigation and can be explained assuming a Mg-Te force constant (k) linear in x. The uncertainty in identifying the ^{24}Mg peak for $0.1 < x < 0.9$ can be significantly decreased if a monoisotopic impurity were used, in turn permitting higher order effects in the x dependence of k to be discovered, e.g., bowing.

Analogous to the effect of host disorder induced broadening in the ternary $Cd_{1-x}Zn_xTe$ associated with the distributions of Cd and Zn in the next nearest neighbor sites, one can examine if the isotopic disorder of the NN's influences the local mode in the binaries. When observed under very high resolution (0.02 cm^{-1}), a reproducible fine structure in the local mode is indeed observed. Other examples of host isotope disorder induced fine structure in the local mode include those for substitutional Si and C in GaAs (Ref. 24) and interstitial oxygen in silicon[25] and germanium.[26,27] Figure 5 shows the fine structure of the ^{24}Mg fundamental in ZnTe; while we have not assigned each peak to a specific isotopic combination, one expects to see many lines due to the various combinations of Te isotopes, and the lifting of the degeneracy whenever the site symmetry is lowered due to the four Te's not being the same isotope. It should be noted, however, that the abundances of the Te isotopes[28] increase with atomic mass causing the line shape to skew toward the low frequency side, as is indeed observed. Such fine structure information can thus be very useful for establishing the substitutional site of unknown impurities. The fine structure of the ^{25}Mg and ^{26}Mg local modes in CdSe for $\mathbf{E} \parallel \hat{c}$ and $\mathbf{E} \perp \hat{c}$ are shown in Figs. 6(a) and 6(b), respectively. While this fine structure, which originates in the random distribution of NN Se isotopes, is identical for the Mg isotopes in a given polarization, there is a marked difference between $\mathbf{E} \parallel \hat{c}$ and $\mathbf{E} \perp \hat{c}$. It should also be noted that the unknown line labeled by a question mark in Fig. 6(a) and its counterpart in $\mathbf{E} \perp \hat{c}$ occurring at 271.4 cm^{-1} (not shown) are devoid of any fine structure. The fine structure associated with the host isotopes was not displayed in the overtones. Their observation, however, required significantly higher concentrations and hence could plausibly result in line broadening leading to the obliteration of the fine structure. At the higher concentrations, this fine structure, even in the fundamental, was replaced by a broad envelope. One could but wish to study the local modes in isotopically pure hosts.

ACKNOWLEDGMENT

The authors acknowledge support from National Science Foundation (Materials Research Group) Grant No. 92-21390.

[1] A. S. Barker and A. J. Sievers, Rev. Mod. Phys. **47**, 2 (1975).
[2] R. C. Newman, Adv. Phys. **18**, 545 (1969).
[3] E. Oh, C. Parks, I. Miotkowski, M. D. Sciacca, A. J. Mayur, and A. K. Ramdas, Phys. Rev. B **48**, 15 040 (1993).
[4] A. Manabe, Y. Ikuta, A. Mitsuishi, H. Komiya, and S. Ibuki, Solid State Commun. **9**, 1499 (1971).
[5] W. Hayes and A. R. L. Spray, J. Phys. C **2**, 1129 (1969).
[6] S. Nakashima, T. Fukumoto, A. Mutsuishi, and K. Itoh, J. Phys. Soc. Jpn. **35**, 1437 (1973).
[7] H. Harada and S. Narita, J. Phys. Soc. Jpn. **30**, 1628 (1971).
[8] A. Manabe, A. Mitsuishi, H. Komiya, and S. Ibuki, Solid State Commun. **12**, 337 (1973).
[9] R. J. Elliott, W. Hayes, G. D. Jones, H. F. MacDonald, and C. T. Sennett, Proc. R. Soc. London Ser. A **289**, 1 (1965).
[10] R. S. Leigh and R. C. Newman, Semicond. Sci. Technol. **3**, 84 (1988). See, also, D. G. Thomas and J. J. Hopfield, Phys. Rev. **150**, 680 (1966).
[11] G. F. Koster, J. O. Dimmock, R. G. Wheeler, and H. Statz, *Properties of the Thirty-Two Point Groups* (MIT Press, Cambridge, MA, 1966).
[12] We have found several errors in the coefficients which are quoted in Ref. 8, and believe the correct values to be given in Table I.
[13] BOMEM, Inc., 450 St-Jean Baptiste, Quebec, Canada G2E 5S5.
[14] Infrared Laboratories, Inc., 1808 E. 17th. Street, Tucson, AZ 85719.
[15] Janis Research Company, Inc., 2 Jewel Drive, Wilmington, MA 01887-0896.
[16] I. Miotkowski (unpublished).
[17] J. Emsley, *The Elements* (Oxford University Press, Oxford, England, 1991).
[18] A. J. Mayur, M. D. Sciacca, I. Miotkowski, G. C. La Rocca, A. K. Ramdas, and S. Rodriguez, Solid State Commun. **91**, 785 (1994).
[19] The derivation leading to Eq. (9) is identical to the argument developed by L. Nordheim, Ann. Phys. (Leipzig) **9**, 607 (1931) in the context of resistivity of binary alloys of metals. It is reproduced in H. Jones, *Encyclopedia of Physics*, edited by S. Flügge (Springer-Verlag, Heidelberg, 1956), Vol. 19, p. 227.
[20] Y. Cai and M. F. Thorpe, Phys. Rev. B **46**, 15 879 (1992).
[21] D. L. Peterson, A. Petrou, W. Giriat, A. K. Ramdas, and S. Rodriguez, Phys. Rev. B **33**, 1160 (1986)
[22] E. Oh, R. G. Alonso, I. Miotkowski, and A. K. Ramdas, Phys. Rev. B **45**, 10 934 (1992).
[23] W. Hayes and H. F. MacDonald, Proc. R. Soc. London Ser. A **297**, 503 (1967).
[24] W. M. Theis, K. K. Bajaj, C. W. Litton, and W. G. Spitzer, Appl. Phys. Lett. **41**, 70 (1982); R. S. Leigh and R. C. Newman, J. Phys. C **15**, L1045 (1982).
[25] B. Pajot and J. P. Deltour, Infrared Phys. **7**, 195 (1967).
[26] B. Pajot and P. Clauws, in *The Proceedings of the 18th International Conference on the Physics of Semiconductors*, edited by O. Engström (World Scientific, Singapore, 1987), p. 911.
[27] A. J. Mayur, M. D. Sciacca, M. K. Udo, A. K. Ramdas, K. Itoh, J. Wolk, and E. E. Haller, Phys. Rev. B **49**, 16 293 (1994).
[28] Tellurium isotopes and their natural abundances (in percent) from Ref. 17 are ^{120}Te:(0.096), ^{122}Te:(2.60), ^{123}Te:(0.908), ^{124}Te:(4.816), ^{125}Te:(7.18), ^{126}Te:(18.95), ^{128}Te:(31.69), and ^{130}Te:(33.80).